



Communication

Investigation of large dielectric permittivity and relaxation behavior of DyMnO₃ single crystalMoumita Patra^a, Arindam Midya^{b,*}, Prabhat Mandal^c^a Department of Physics, Raghunathpur College, Raghunathpur, Purulia 723133, India^b Department of Physics, City College, 102/1, Raja Rammohan Sarani, Kolkata 700009, India^c Saha Institute of Nuclear Physics, HBNI, 1/AF Bidhannagar, Kolkata 700064, India

ARTICLE INFO

Communicated by Sanyal Milan K

Keywords:

Perovskite
Dielectric relaxation
Maxwell–Wagner effect
Second ionization

ABSTRACT

We have investigated the frequency-dependent dielectric properties of DyMnO₃ single crystal in the temperature region from 100 K to 320 K. The material shows a large dielectric permittivity in the low-frequency range around room temperature. The dielectric permittivity exhibits a strong temperature dependence at all frequency and two anomalies which can be associated with the Debye-type relaxation with activation energies of 0.66 eV and 0.23 eV in the higher (around 300 K) and lower (around 150 K) temperature regions, respectively. The high value of activation energy around room temperature suggests that the relaxation is associated to the charge carriers hopping resulting from the second ionization of oxygen vacancies. However, the impedance analysis suggests that the low-temperature relaxation is due to the Maxwell–Wagner type effects originating from the dipoles at the surface.

1. Introduction

For the past few decades, perovskite manganites RMnO₃ (where R = Rare earth elements) have been a subject of great interest for both the technological application as well as to develop theoretical understanding of the complex mechanism of various coupled ordering phenomena. Firstly, the presence of different functional properties like magnetoresistance, magnetocaloric effect, multiferroicity, large dielectric constant, makes the manganites promising material for multifunctional device such as magnetic memory device, spintronic application, magnetic refrigeration, etc [1–5]. Secondly, being a class of complex oxides with rich phase diagram and various coupled ordering phenomena, it is a potential system to achieve a clear theoretical understanding [6–8].

These multifunctional rare-earth manganites having very rich phase diagram often show structural phase transition, as a result, various interesting properties are observed around the transition temperature. Generally, RMnO₃ crystallizes either in orthorhombic or hexagonal structure depending on the rare-earth ionic radius [9,10]. The compounds with larger rare earth ion (R = Tb, Dy) crystallize in orthorhombic structure, whereas hexagonal structure is more stable for smaller ionic radius of R (R = Ho to Lu, Y) though they can be synthesized in orthorhombic structure by applying different growth conditions [11].

Recent studies on dielectric properties of RMnO₃ can be divided into two branches where some studies were concentrated on the multiferroicity of hexagonal RMnO₃ (R = Y, Ho, Er, Tm, Yb, Lu, and

Sc) family [10,12]. On the other hand, orthorhombically distorted perovskite rare-earth manganites RMnO₃ (R = Tb, Dy) was reported to exhibit gigantic and intrinsic magnetoelectric couplings [1,13]. However, the origin of dielectric relaxation remains unclear in both types of RMnO₃. For example, in polycrystalline TbMnO₃, it is claimed that high-temperature relaxation is due to the internal barrier-layer capacitor effect, whereas the low-temperature relaxation was ascribed to the dipolar effect induced by charge-carrier-hopping motions inside the grains [14]. In case of HoMnO₃ thin film, those behaviors were explained in terms of the hopping conductivity and the dipolar effect induced by the charge carriers [11]. Reports on the dielectric relaxation of polycrystalline YMnO₃ suggest that, hopping or space charge polarization through electrically inhomogeneous structure resulting from grain/grain boundary interfaces is responsible for this behavior [15,16]. Whereas the detail study on YMnO₃ single crystals suggests that the low-temperature relaxation is due to the Maxwell–Wagner type effect while the high temperature one is originated from hopping of charge carriers resulting from the second ionization of oxygen vacancies [10].

Recently, from the study of the temperature dependent dielectric/impedance spectroscopy of polycrystalline DyMnO₃, Yang et al. and Wang provided a new insight into the dielectric properties. They have correlated the low-temperature relaxation process to short-range polaronic variable-range-hopping induced dipolar-type relaxation in

* Corresponding author.

E-mail address: arindam.midya@citycollegekolkata.org (A. Midya).

grains, whereas the high-temperature one is to the Maxwell–Wagner relaxation at grain boundary/interfaces [9,17].

In this work, we have investigated the dielectric relaxation of the single crystalline DyMnO₃ to get the insight into the dielectric behavior in the temperature region 100 K–320 K. The material shows a large dielectric permittivity of the order of 10⁴ in the low-frequency range around room temperature and two dielectric anomalies: one around 300 K and another around 150 K. Though all these features in polycrystalline DyMnO₃ have been attributed to the interfaces between the grains and the grain boundaries, it cannot be the possible origin as we have studied the dielectric properties in single crystalline material and observe a Maxwell–Wagner (MW) type relaxation around 100 K to 225 K similar to that observed in single crystalline YMnO₃. We suggest that the low-temperature relaxation process in this system is originated from the dipoles at the surface and the feature present around 300 K can be related to the hopping of charge carriers resulting from the second ionization of oxygen vacancies as in the case of YMnO₃ single crystal [10].

2. Experimental details

Initially, single phase polycrystalline DyMnO₃ sample was prepared following the standard solid-state reaction method. Stoichiometric amount of high purity Dy₂O₃ and Mn₂O₄ were mixed thoroughly and the mixture was heated at 1100 °C for 15 h. Then, the material was reground and heated again at 1200 °C for 24 h. The product was reground into fine powder to make two ceramic rods of 4–8 cm in length and about 6 mm in diameter for crystal growth by filling it into rubber tubes and subjecting them to a hydrostatic pressure of 60 MPa. These cylindrical rods were sintered at 1350 °C for 15 h prior to growth. During the polycrystalline sample preparation, we used a uniform heating and cooling rates of 120 °C/h. Single crystal was grown from these polycrystalline rods by traveling solvent floating zone technique using an image furnace (NEC SC-M15HD). In this method, the radiation from four infrared lamps is focused at their common focal point to melt the junction of the ceramic seed and feed rods of DyMnO₃. Unlike the flux growth and chemical vapour transport techniques, the floating zone is a non-contact method and there is no scope to record the temperature profile of crystal growth. During the growth, the seed and feed rods were rotated at 25 rpm in opposite directions. At a growth rate of 4–5 mm/h, crystal of typical dimensions 3–4 cm length and 4–5 mm diameter was obtained. Growth was performed in the air ambience.

The crystal structure of the grown sample was determined by X-ray diffraction (XRD) of powdered sample at room temperature by an x-ray diffractometer with CuK_α radiation. Diffraction pattern was recorded in the range 20–90 degree (2θ) with 0.02 degree step size and 2 s per step. The orientation of the single crystalline samples has been confirmed from the magnetic susceptibility measurement as described in our earlier report [18]. For the dielectric measurements, as prepared samples have been cut into a piece with dimensions 6 mm × 9 mm as shown in the left inset of Fig. 1 and silver paste was applied to this piece to form a parallel-plate capacitor. The temperature and frequency dependence of dielectric properties were measured using Wayne Kerr 6500B impedance analyzer (Wayne Kerr Electronic Instrument Co.). Data were taken in the frequency range of 20 Hz–1 MHz from 100 K to 320 K with signal amplitude of 50 mV. Sample temperature was controlled using a temperature controller (Lakeshore 340) in a liquid nitrogen cryostat.

3. Results and discussion

Fig. 1 shows the room temperature XRD pattern of the powdered sample along with the fitting using Rietveld analysis. From the figure, we see that the experimental data can be fitted well with the *Pnma* orthorhombic structure. The results obtained from the Rietveld

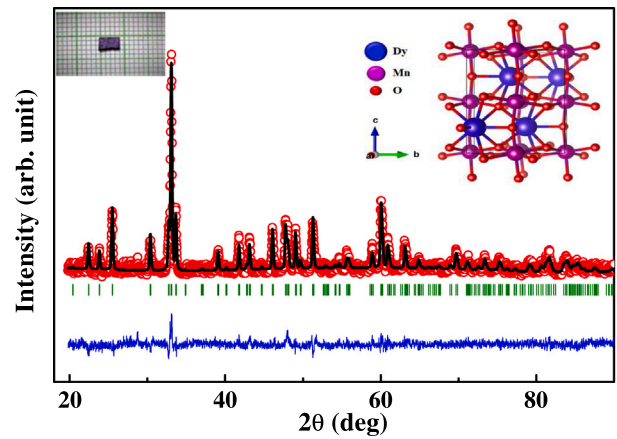


Fig. 1. Room temperature observed and Rietveld refined powder XRD pattern of DyMnO₃. The Bragg position and the difference between the observed and calculated patterns are plotted at the bottom. Left inset shows the typical dimension of the sample for dielectric measurement and right inset shows the crystal structure of DyMnO₃.

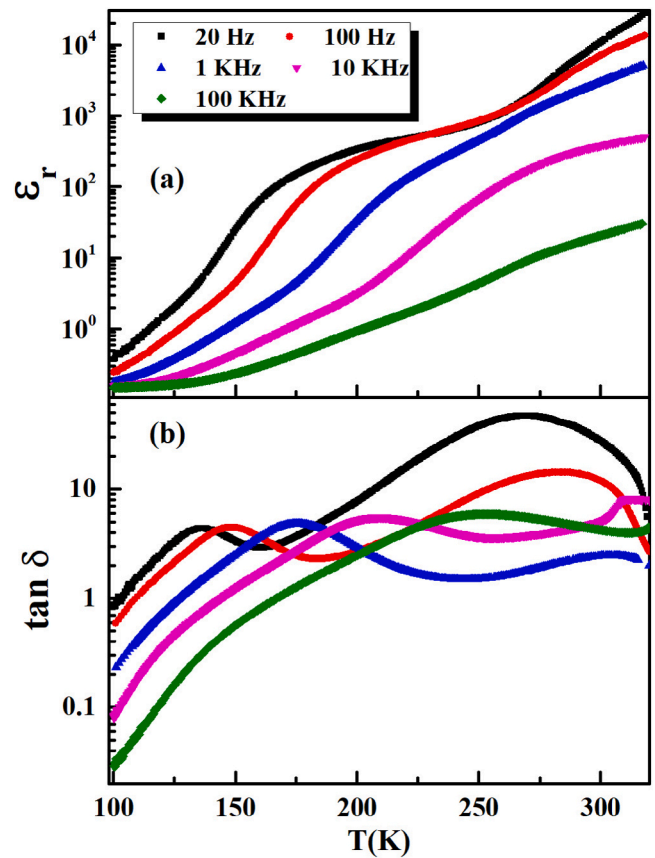


Fig. 2. Temperature dependence of (a) dielectric constant and (b) dielectric loss of DyMnO₃ single crystal at various frequencies.

refinement are listed in Table 1 which are in accordance with the previously reported results [19]. The calculated bulk crystalline density as estimated from the XRD analysis is 7.74 g/cc. The crystal structure of DyMnO₃ has been shown in the inset of Fig. 1.

Fig. 2(a) shows the temperature dependence of the dielectric permittivity ϵ_r at different frequencies. As the temperature increases, ϵ_r increases up to a particular temperature, then a saturation-like behavior starts to appear. Upon further increase in temperature, ϵ_r increases up to the highest measured temperature. With increasing frequency, the

Table 1

Structural parameters obtained from the Rietveld refinement of the XRD pattern for DyMnO₃ sample.

Atoms	x	y	z
Dy	0.01403	0.08075	0.25000
Mn	0.50000	0	0
O1	0.11365	0.47453	0.25000
O2	0.69533	0.31099	0.04813
Cell dimensions	a(Å)	b(Å)	c(Å)
	5.2834(3)	5.8358(3)	7.3895(4)
R _p = 12	R _{wp} = 16	R _{exp} = 11.8	χ ² = 1.97

magnitude of ϵ_r decreases and the temperature at which the saturation starts to appear, shifts toward the higher temperature. Overall, these features indicate a relaxor-type behavior.

Thermal variation of dielectric loss ($\tan \delta$) at different frequencies is shown in Fig. 2(b). $\tan \delta$ vs T shows two distinct anomalies in our measured temperature range. These two anomalies shift towards the higher temperature side with increasing frequency, indicating a thermally activated charge dynamics. In general, for a thermally activated relaxation process, the temperature dependence of the relaxation time can be described in terms of the Arrhenius relation,

$$\tau = \tau_0 \exp[E_a/k_B T], \quad (1)$$

where τ_0 , E_a and k_B are the relaxation time at infinite temperature, activation energy and Boltzmann constant, respectively. At peak position ($T = T_p$), we get,

$$\ln(\omega\tau) = 0 \quad (2)$$

Using Eqs. (1) and (2), we can write,

$$\ln(2\pi f \tau_0) + E_a/k_B T = 0. \quad (3)$$

One can estimate the activation energy for the dielectric relaxation from the above equation. In order to understand the mechanism of dielectric relaxation, we have calculated the activation energy from the $\ln(f)$ versus $1000/T_p$ curves (Fig. 3) for both the regions separately. It can be seen that the slope as well as the intercept are very different for the lower and higher temperature regions which suggest different mechanisms for these two regions. The activation energy E_a and relaxation time at infinite temperature τ_0 in the low-temperature region can be estimated as 0.23 ± 0.05 eV and 4.44×10^{-11} s which are in good agreement with the previously reported results (0.24 eV) for polycrystalline DyMnO₃ [9,17]. The low value of activation energy could be related to the universal Maxwell–Wagner relaxation due to a complex surface phenomenon as described in polycrystalline DyMnO₃ and also for single crystalline YMnO₃. However, the values of E_a and τ_0 which have been estimated from the Arrhenius plot around room temperature are 0.66 ± 0.03 eV and 0.9×10^{-13} s respectively. The estimated value of E_a is different from that reported (0.32 eV) by Wang for polycrystalline DyMnO₃ [17]. Rather it is closer to the value (0.66 eV) for the single crystalline YMnO₃ in the high temperature region. E_a in the range of 0.6–1.2 eV has also been observed for Pb-based perovskite ferroelectrics and Sr_{1-1.5x}Bi_xTiO₃ where it is associated with the double-ionized oxygen vacancies [20,21]. Therefore, we suggest that in this region, the hopping entities are electrons resulting from the second ionization of oxygen vacancies.

The Cole–Cole equation is a relaxation model that is often used to get insight into the dielectric relaxation for these types of systems. According to this model, the complex dielectric permittivity can be written as,

$$\epsilon(\omega) = \epsilon_\infty + \frac{\epsilon_s - \epsilon_\infty}{1 + (i\omega\tau)^{1-\alpha}}, \quad (4)$$

where ϵ_s and ϵ_∞ are the static and infinite frequency dielectric permittivity, ω is the angular frequency and τ is a time constant. The exponent

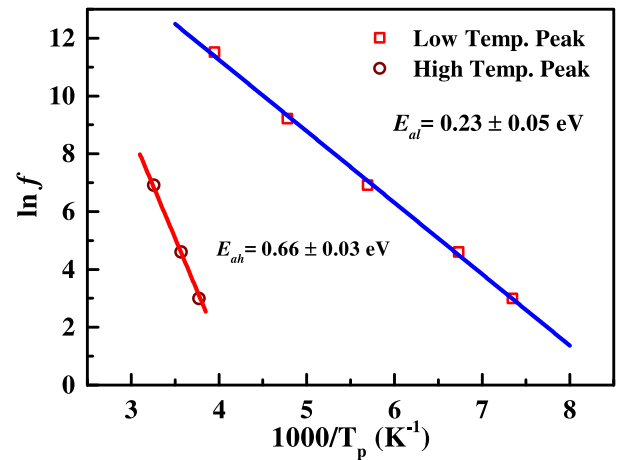


Fig. 3. Arrhenius plots for relaxations of DyMnO₃ single crystal for two different temperature regions.

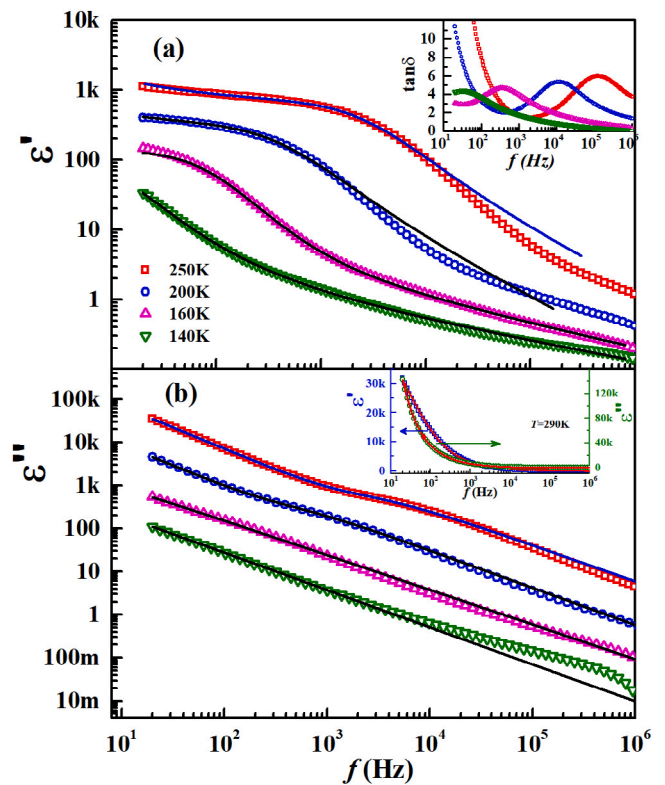


Fig. 4. Frequency dependences of (a) ϵ' and (b) ϵ'' at various temperatures for DyMnO₃ single crystal. The solid lines represent the best fits to Eqs. (5) and (6) respectively, which include both a Cole–Cole relaxation and a complex conductivity contribution. Inset of (a) shows the frequency dependence of $\tan \delta$ at different temperatures and the inset of (b) shows Frequency dependences of ϵ' (left y-axis) and ϵ'' (right y-axis) at 290 K.

α describes different spectral shapes, which can take any value between 0 and 1. Furthermore, an electrical conductivity term ($\frac{\sigma}{\epsilon_0\omega^s}$) is added to the relaxation Eq. (4), when the electrical conductivity is large, σ is the complex conductivity and s is a constant and it can have a value between 0 and 1 [22,23]. The complex permittivity, after adding the conductivity term, may be decomposed into real and imaginary parts as,

$$\epsilon'(\omega) = \epsilon_\infty + \frac{(\epsilon_s - \epsilon_\infty)[1 + (\omega\tau)^{1-\alpha} \sin(\alpha\pi/2)]}{1 + 2(\omega\tau)^{1-\alpha} \sin(\alpha\pi/2) + (\omega\tau)^{2-2\alpha}} + \frac{\sigma_2}{\epsilon_0\omega^s} \quad (5)$$

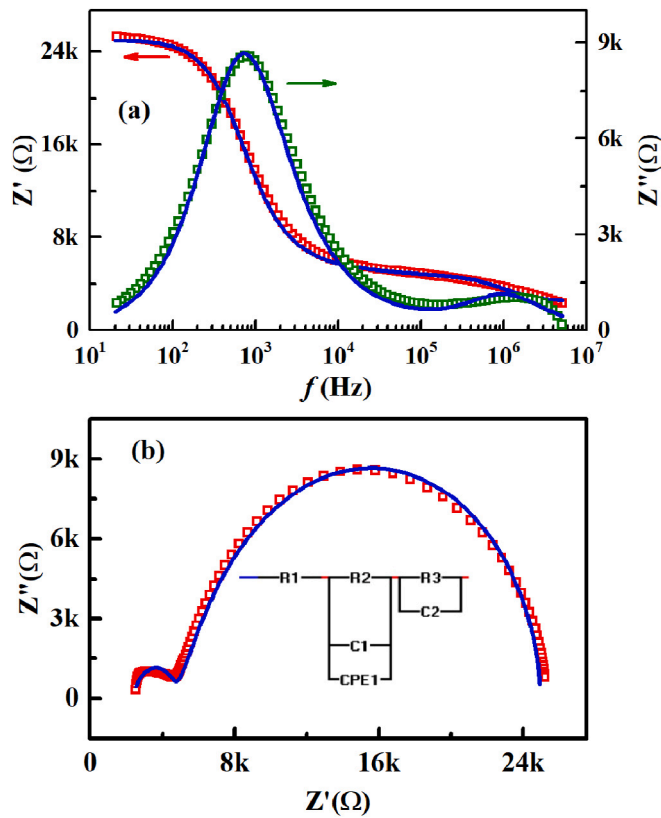


Fig. 5. (a) Frequency dependences of Z' and Z'' at 250 K (b) Nyquist plot of complex impedance at 250 K. Insets in (b) depicts the equivalent circuit model. Solid lines in (a) and (b) are the results of the equivalent circuit model fitting.

and

$$\epsilon''(\omega) = \frac{(\epsilon_s - \epsilon_\infty)(\omega\tau)^{1-\alpha} \cos(\alpha\pi/2)}{1 + 2(\omega\tau)^{1-\alpha} \sin(\alpha\pi/2) + (\omega\tau)^{2-2\alpha}} + \frac{\sigma_1}{\epsilon_0\omega^s}, \quad (6)$$

where σ_1 is the conductivity due to the free charge carrier and σ_2 is the conductivity due to the space charges.

Frequency dependence of real (ϵ') and imaginary component (ϵ'') of dielectric permittivity have been shown in Fig. 4(a) and (b) respectively. The real part shows a step-like behavior whereas the imaginary part decreases monotonically with increase in frequency. However, both the parts are weakly dependent on temperature in higher frequency region. As shown in the inset of Fig. 4(a), the frequency dependence of $\tan \delta$ plot shows a distinct peak which can be associated with the step-like dielectric permittivity. We have analyzed the frequency dependence of dielectric data using the Eqs. (5) and (6). The fitting results using Eqs. (5) and (6) are shown with the solid lines in Figs. 4(a) and 4(b), respectively. The parameters obtained from the best fitting are summarized in Table 2 at different temperatures. We found that except at high frequency, $\epsilon(\omega)$ fitted well with the experimental data for both $\epsilon'(\omega)$ and $\epsilon''(\omega)$. As shown in the table, ϵ_s and ϵ_∞ increase with increasing temperature but the exponent α is almost independent of temperature and the value is ~ 0.17 . The small value of α suggests a Debye like nature of relaxation because the Cole–Cole model reduces to the Debye model for $\alpha = 0$. The inset of Fig. 5(b) shows the frequency dependence of dielectric data at 290 K along with the fitting using Eqs. (5) and (6). The value of τ_0 has been estimated using Eq. (1) and from the τ value obtained from fitting as 0.2×10^{-12} s which is a good agreement with the values $0.5 - 7 \times 10^{-12}$ s observed by Ang et al. [20].

In order to search the origin of the low-temperature relaxation behavior for single crystalline YMnO_3 , it is concluded from the electrode dependence low-frequency dielectric constant that electrode–sample

Table 2

ϵ_s , ϵ_∞ , α and s obtained from the best fitting with the modified Cole–Cole relaxation for DyMnO_3 .

T(K)	ϵ_s	ϵ_∞	α	s
140	7 ± 0.2	0.1 ± 0.04	0.18 ± 0.006	0.89 ± 0.003
160	70 ± 1	0.1 ± 0.009	0.17 ± 0.003	0.96 ± 0.0001
200	300 ± 3	0.2 ± 0.02	0.16 ± 0.004	0.98 ± 0.0008
250	919 ± 4.1	0.5 ± 0.06	0.18 ± 0.001	0.99 ± 0.0002

interface dipoles govern the low-frequency response [10]. Now, we analyze the impedance spectra at different temperatures in the low-temperature region. Fig. 5(a) and (b) show one representative complex impedance spectra for DyMnO_3 single crystal at 250 K. The spectrum has been resolved into two semicircles, and dielectric response may be attributed to the combined effect of bulk at high frequency (small semicircle) and interfaces at low frequency (large semicircle). Large semicircle at low frequency is due to the different electrical conductivities of bulk and the electrode, the charge carriers would be localized and accumulated at the interfaces of the bulk and the electrode surfaces under an external ac field. This type of process could give rise to MW interfacial relaxation [24,25] known as extrinsic effect. Whereas the small semicircle at high frequency is the intrinsic dielectric responses arising from the bulk DyMnO_3 single crystal. The dielectric response is described by equivalent circuit model, as shown in the inset of Fig. 5(b), which is in the frame of MW model and it is composed of series of two circuits, one with parallel interfaces resistance (R_3) and a capacitance (C_2) and the other with parallel bulk resistance (R_2), capacitance (C_1), and constant phase element (CPE1). The equivalent circuit model fits well with the experimental data at 250 K. Values of the best fitting parameters are $R_1 = 2.4 \text{ k}\Omega$, $R_3 = 20.5 \text{ k}\Omega$, $C_2 = 10.6 \text{ nF}$, $R_2 = 2 \text{ k}\Omega$, $C_1 = 71.1 \text{ pF}$. We have calculated the activation energy (E_a) from the temperature dependent interfacial resistance (R_3) in the region from 120 K to 250 K. The activation energy estimated from the relation ($\rho = \rho_0 \exp(E_a/k_B T)$) is 0.2 eV which is close to the value estimated from the Arrhenius plot.

4. Conclusion

In conclusion, we have concentrated to determine the origin of the dielectric relaxation behavior of orthorhombic DyMnO_3 single crystal in the temperature range between 150 K and 320 K using frequency-dependent dielectric measurements. The material exhibits a large dielectric permittivity in the low-frequency range around room temperature which makes the material suitable for optical applications but high values of $\tan \delta$ makes it little disadvantageous. Two different anomalies are present in the measured temperature region. The behavior associated with lower-temperature region can be related to the Maxwell–Wagner relaxation mechanism due to a complex surface phenomenon. And the hopping of charge carriers resulting from second ionization of oxygen vacancies is responsible for the relaxation anomalies around room temperature.

Declaration of competing interest

The authors declare that they have no known competing financial interests or personal relationships that could have appeared to influence the work reported in this paper.

Data availability

The data that support the findings of this study are available from the corresponding author upon reasonable request.

References

- [1] T. Kimura, T. Goto, H. Shintani, K. Ishizaka, T. Arima, Y. Tokura, *Nature* 426 (2003) 55–58.
- [2] M. Bibes, A. Barthélemy, *Nature Mater.* 7 (2008) 425–426.
- [3] Z.J. Huang, Y. Cao, Y.Y. Sun, Y.Y. Xue, C.W. Chu, *Phys. Rev. B* 56 (1997) 2623.
- [4] B. Lorenz, A.P. Litvinchuk, M.M. Gospodinov, C.W. Chu, *Phys. Rev. Lett.* 92 (2004) 087204.
- [5] M. Fiebig, T. Lottermoser, D. Fröhlich, A.V. Goltsev, R.V. Pisarev, *Nature* 419 (2002) 818–820.
- [6] M. Gajek, M. Bibes, S. Fusil, K. Bouzehouane, J. Fontcuberta, A. Barthélemy, A. Fert, *Nature Mater.* 6 (2007) 296–302.
- [7] W. Eerenstein, N.D. Mathur, J.F. Scott, *Nature* 442 (2006) 759–765.
- [8] W. Prellier, M.P. Sing, P. Murugavel, *J. Phys.: Condens. Matter* 17 (2005) R803.
- [9] J. Yang, J. He, J.Y. Zhu, W. Bai, L. Sun, X.J. Meng, X.D. Tang, C.-G. Duan, D. Remiens, J.H. Qiu, J.H. Chu, *Appl. Phys. Lett.* 101 (2012) 222904.
- [10] U. Adem, N. Mufti, A.A. Nugroho, G. Catalan, B. Noheda, T.T.M. Palstra, *J. Alloys Compd.* 638 (2015) 228–232.
- [11] W. Wanga, D. Yuan, Y. Sun, Y. Sun, *J. Appl. Phys.* 106 (2009) 024106.
- [12] A.S. Gibbs, K. Knight, P. Lightfoot, *Phys. Rev. B* 83 (2011) 094111.
- [13] F. Schrettle, P. Lunkenheimer, J. Hemberger, V.Y. Ivanov, A.A. Mukhin, A.M. Balbashov, A. Loidl, *Phys. Rev. Lett.* 102 (2009) 207208.
- [14] C.C. Wang, Y.M. Cui, L.W. Zhang, *Appl. Phys. Lett.* 90 (2007) 012904.
- [15] P. Ren, H. Fan, X. Wang, *Appl. Phys. Lett.* 103 (2013) 152905.
- [16] M. Tomczyk, P.M. Vilarinho, A. Moreira, A. Almeida, *J. Appl. Phys.* 110 (2011) 064116.
- [17] W.T. Wang, *Korean J. Mater. Res.* 29 (2019) 753–756.
- [18] A. Midya, S.N. Das, P. Mandal, S. Pandya, V. Ganesan, *Phys. Rev. B* 84 (2011) 235127.
- [19] S. Harikrishnan, S. Rößler, C.M.N. Kumar, H.L. Bhat, U.K. Rößler, S. Wirth, F. Steglich, S. Elizabeth, *J. Phys. Condens. Mater.* 21 (2009) 96002.
- [20] C. Ang, Z. Yu, L.E. Cross, *Phys. Rev. B* 62 (2000) 228.
- [21] A. Peláiz-Barranco, J.D.S. Guerra, R. López-Noda, E.B. Araújo, *J. Phys. D: Appl. Phys.* 41 (2008) 215503.
- [22] D. Ming, J.M. Reau, J. Ravez, J. Gitae, P. Hagenmuller, *J. Solid State Chem.* 116 (1995) 185–192.
- [23] B.S. Kang, S.K. Choi, C.H. Park, *J. Appl. Phys.* 94 (2003) 1904.
- [24] M. Kawarasaki, K. Tanabe, I. Terasaki, Y. Fujii, H. Taniguchi, *Sci. Rep.* 7 (2017) 1–6.
- [25] Y. Song, X. Wang, Y. Sui, Z. Liu, Y. Zhang, H. Zhan, B. Song, Z. Liu, Z. Lv, L. Tao, J. Tang, *Sci. Rep.* 6 (2016) 1–8.